SPIE Smart Structure and Materials + Nondestructive Evaluation and Health Monitoring 2010,
Sensors and Smart Structures Technologies for Civil, Mechanical, and Aerospace Systems,
San Diego, CA, 7 - 11 March, 2010, paper # SS10-7647-97

Modeling of Power and Energy Transduction of Embedded Piezoelectric Wafer Active Sensors for Structural Health Monitoring

Bin Lin, Victor Giurgiutiu
Mechanical Engineering Department, University of South Carolina
Columbia, SC 29208, linbin@cec.sc.edu, victorg@sc.edu

ABSTRACT

This paper presents a systematic investigation of power and energy transduction in piezoelectric wafer active sensors (PWAS) for structural health monitoring (SHM). After a literature review of the state of the art, the paper develops a simplified pitch-catch model of power and energy transduction of PWAS attached to structure. The model assumptions include: (a) 1-D axial and flexural wave propagation; (b) ideal bonding (pin-force) connection between PWAS and structure; (c) ideal excitation source at the transmitter PWAS and fully-resistive external load at the receiver PWAS. Frequency response functions are developed for voltage, current, complex power, active power, etc.

First, we examined PWAS transmitter and determined the active power, reactive power, power rating of electrical requirement under harmonic voltage excitation. It was found that the reactive power is dominant and defines the power requirement for power supply / amplifier for PWAS applications. The electrical and mechanical power analysis at the PWAS structure interface indicates all the active electrical power provides the mechanical power at the interface. This provides the power and energy for the axial and flexural waves power and energy that propagate into the structure. The sum of forward and backward wave power equals the mechanical power PWAS applied to the structure. The parametric study of PWAS transmitter size shows the proper size and excitation frequency selection based on the tuning effects.

Second, we studied the PWAS receiver structural interface acoustic and electrical energy transduction. The parametric study of receiver size, receiver impedance and external electrical load gives the PWAS design guideline for PWAS sensing and power harvesting applications.

Finally we considered the power flow for a complete pitch-catch setup. In pitch-catch mode, the power flows from electrical source into piezoelectric power at the transmitter; the piezoelectric conduction converts the electrical power into the mechanical interface power at the transmitter PWAS and then into the acoustic wave power travelling in the structure. The wave power arrives at the receiver PWAS and is captured at the mechanical interface between the receiver PWAS and the structure; the captured mechanical power is converted back into electrical power at the receiver PWAS and measured by the receiver electrical instrument. Our numerical simulation and graphical chart show the trends in the power and energy flow behavior with remarkable peaks and valleys that can be exploited for optimum design.

Keywords: frequency response function, power, energy, piezoelectric wafer active sensors

1. INTRODUCTION

1.1 Background

The mounting costs of maintaining our aging infrastructure and the associated safety issues are a growing national concern. Over 27% of our nation's bridges are structurally deficient of functionally obsolete[1]. Deadly accidents are still marring our everyday life. In response to these growing concerns, structural health monitoring (SHM) sets forth to determine the health of a structure by monitoring over time a set of structural sensors and assessing the remaining useful

life and the need for structural actions. Built-in SHM system capable of detecting and quantifying damage would increase the operational safety and reliability, would conceivably reduce the number of unscheduled repairs, and would bring down maintenance cost.

The type and efficiency of the SHM sensors play a crucial role in the SHM system success. Ideally, SHM sensors should be able to actively interrogate the structure and find out its state of health, its remaining life, and the effective margin of safety. Essential in this determination is to find out the presence and extend of structural damage. Recent SHM work has shown that piezoelectric wafers adhesively bonded to the structure successfully emulate the NDE methodology (pitch-catch, pulse-echo, phased array, Figure 1) while being sufficiently small and inexpensive to allow permanent attachment to the monitored structure. Piezoelectric wafer active sensors (PWAS) are small, lightweight, unobtrusive, and inexpensive and achieve direct transduction between electric and elastic wave energies. Two SHM sensing principles can be considered: (a) passive SHM sensing, in which the damage of the structure is inferred from the changes in load and strain distributions measured by the sensors; and (b) active SHM sensing, in which the damage is sensed by active interrogation of the structure with elastic waves. The power and energy flow in active and passive sensing is an import factor and has not systematically addressed.

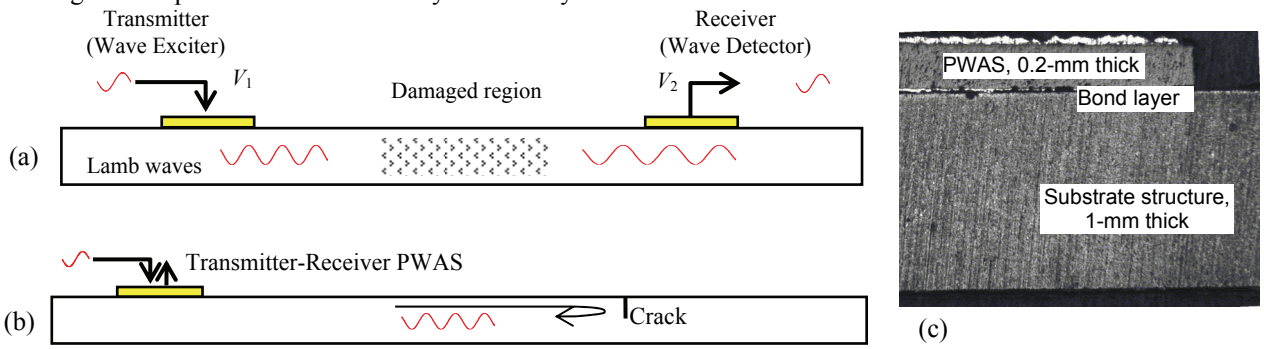

Figure 1 (a) pitch-catch method; (b) pulse-echo method; (c) boded interface between PWAS and structure

1.2 State of the Art

Up to date work on PWAS SHM technology has not yet systematically addressed the modeling of power and energy transduction. However, this topic has been addressed to a certain extent in classical NDE [2-5]. Viktorov [2] mentioned the transmissibility function between an NDE transducer and the guided waves in the structure, but did not give an analytical expression but rather relies on experimentally determination. Auld [3] treated comprehensibly the power and energy of ultrasonic acoustic fields and developed the complex reciprocity approach to their calculation. He developed some predictive models for surface acoustic wave (SAW) devices that relied on the simplifying assumption of single mode nondispersive Rayleigh wave propagation. Rose [5] developed a model for coupling between an angle-beam ultrasonic transducer and a system of guided Lamb waves in the structure using the normal modes expansion approach. However, this model was not specific about how the shear transfer takes place through the gel coupling between the transducer and the structure. Classical NDE analysis has not studied in detail the power flow between transducer and structure because (a) the coupling-gel interface did not have clearly predictable behavior; (b) power was not generally an issue, since NDE devices are not meant to operate autonomously on harvested power.

Although not much addressed by classical NDE analysis, the understanding and mastering of the power and energy flow is of paramount importance for the design of autonomous SHM systems employing structurally integrated active sensors.

1.3 Motivation

The purpose of the paper is to develop the analysis methods to understand and master of the power and energy flow in PWAS active and passive SHM sensing. It is important for the design of autonomous SHM systems employing PWAS with optimum power and energy flow. The following issues were addressed: (a) predictive modeling of the frequency response function and the power and energy transduction at the interface between PWAS and the structure in the presence of axial and flexural waves; (b) identification of maximum energy flow; (c) knowing that energy flows under impedance match conditions.

2. FREQUENCY RESPONSE FUNCTION

Frequency response functions (FRF) are developed for voltage, current, complex power, active power, etc in this section. Under harmonic excitation, the FRF is the measure of any system's output spectrum in response to an input signal. In PWAS SHM setup, the input is the excitation voltage, the output might be voltage, current, complex power etc. The analytical model of FRF and power and energy transduction is based on the following assumptions those include: (a) ideal bonding (pin-force) connection between PWAS and structure; (b) ideal excitation source at the transmitter PWAS and fully-resistive external load at the receiver PWAS; (c) 1-D axial and flexural wave propagation. Frequency response functions are developed for voltage, current, complex power, active power, etc.
For compactness, the notation used:

$$\dot{U} = \frac{\partial}{\partial t}U \qquad U' = \frac{\partial}{\partial x}U \qquad U = \hat{U}e^{i\omega t} \qquad \bar{U} = conj(U) \tag{2.1}$$

The notation $\tilde{f}$ is the space domain Fourier transform and $h(t)*x(t)$ is the convolution of two variables

$$\tilde{f}(\xi) = \int_{-\infty}^{\infty} f(x)e^{-i\xi x}dx \qquad \mathcal{F}\{h(t)*x(t)\} = H(\omega)X(\omega) \tag{2.2}$$

2.1 Constitutive Equation

Consider a PWAS of length l, width b and thickness t, undergoing longitudinal expansion, u_1, induced by the thickness polarization electric field, E_3. The electric field is produced by the application of a harmonic voltage $V(t) = \hat{V}e^{i\omega t}$ between the top and bottom surface electrodes. The 1-D piezoelectric constitutive equation is

$$\begin{aligned} S_1 &= s_{11}^E T_1 + d_{31}E_3 \\ D_3 &= d_{31}T_1 + \varepsilon_{33}^T E_3 \end{aligned} \tag{2.3}$$

where S_1 is the strain, T_1 is the stress, D_3 is the electrical displacement, s_{11}^E is the mechanical compliance at zero field, ε_{33}^T is the dielectric constant at zero stress, d_{31} is the induced strain coefficient.

2.2 Pin-force Model

The actuation and sensing between the PWAS and the structure is achieved through the adhesive layer. The adhesive layer act as a shear layer, in which the mechanical effects are transmitted through shear effects. Under static and low-frequency dynamic conditions, the usual hypothesis associates with simple axial and flexural motions, i.e., constant displacement for axial motion and linear displacement strain for flexural motion.

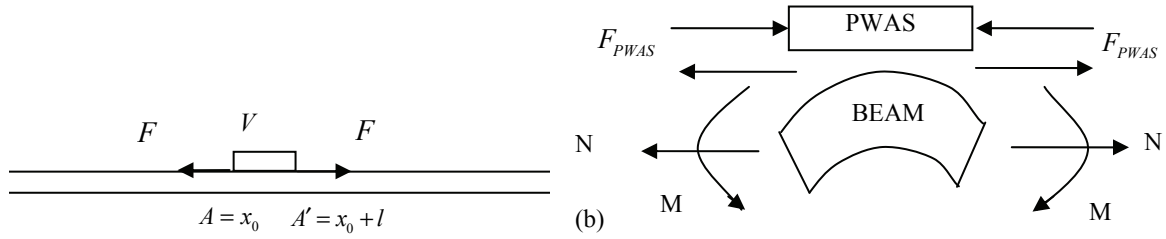

Figure 2 PWAS model (b)PWAS attached on a bar; (b) pin-force model

The shear-lag analysis indicates that, as the bond thickness decrease, the shear stress transfer becomes concentrated over some infinitesimal distances at the ends of the PWAS actuator (Figure 2). The concept of ideal bonding (also known as the pin-force model) assumed that all the load transfer take place over an infinitesimal region at the PWAS ends, and the induced-strain action is assumed to consist of a pair of concentrated forces applied at the ends. The overall axial force and bending moment applied to the structure can be written as

$$N_e(x,t) = \left\{\hat{F}\left[-H(x-x_0) + H(x-x_0-l)\right]\right\}e^{-i\omega t} \tag{2.4}$$

$$M_e(x,t) = -\left\{\frac{h}{2}\hat{F}\left[-H(x-x_0) + H(x-x_0-l)\right]\right\}e^{-i\omega t} \tag{2.5}$$

2.3 PWAS Transmitter and Receiver

The relation between PWAS pin-force and transmitter input voltage and the relation between pin-force and receiver output voltage were established.

Under ideal excitation source at the transmitter PWAS, the relation of the pin-end force and the elongation of PWAS when PWAS was constrained on the structure can be derived from the constitutive equation.

$$\hat{F} = k_i(\Delta\hat{u} - u_{ISA}) \tag{2.6}$$

where k_i and u_{ISA} were defined as the internal stiffness of PWAS actuator and induced displacement respectively, i.e.

$$k_i = \frac{tb}{s_{11}^E l} \qquad u_{ISA} = d_{31}\frac{\hat{V}}{t}l \tag{2.7}$$

Under fully-resistive external load at the receiver PWAS and harmonic dynamic strain excitation, the relation of output voltage and PWAS elongation is

$$\hat{V} = \frac{1}{Y_e + (1-k_{31}^2)Y_0} i\omega b \frac{d_{31}}{s_{11}} \Delta u \tag{2.8}$$

The relation of the pin-force at PWAS receiver and the elongation of PWAS is

$$\hat{F} = R(\omega)k_i\Delta\hat{u} \text{ where } R(\omega) = (1 - \frac{k_{31}^2 Y_0}{Y_e + (1-k_{31}^2)Y_0}) \tag{2.9}$$

2.4 Wave Propagation Method

The axial wave equation under harmonic variation is

$$-\omega^2 u(x,t) - c^2 u''(x,t) = \frac{N_e'}{\rho A} \tag{2.10}$$

Where $c = \sqrt{E/\rho}$ is the axial wave speed and $\xi_0^2 = \omega^2/c^2$ is the wavenumber of axial waves in the 1-D medium. The wave equation can be written as

$$-u'' - \xi_0^2 u = h(x,t) \quad \text{where} \quad h(x,t) = \frac{N_e'(x,t)}{EA} \tag{2.11}$$

The space-domain Fourier transform has property $\tilde{f}' = i\xi\tilde{f}$. Using the space-domain Fourier transform on both sides and the axial wave equation becomes

$$\tilde{u} = \frac{1}{\xi^2 - \xi_0^2}\tilde{h} \quad \text{where} \quad \tilde{h}(\xi) = \int_{-\infty}^{\infty} h(x)e^{-i\xi x}dx = \frac{1}{EA}\int_{-\infty}^{\infty}\left\{\hat{F}\left[-\delta(x-x_0) + \delta(x-x_0-l)\right]\right\}e^{-i\xi x}dx \tag{2.12}$$

Taking the inverse space-domain Fourier transform yields the solution in the space domain. The solution is

$$u(x,t) = \frac{1}{2\pi EA}e^{-i\omega t}\int_{-\infty}^{\infty}\frac{1}{\xi^2 - \xi_0^2}\left[\hat{F}_A(-e^{-i\xi x_0} + e^{-i\xi(x_0+l)})\right]e^{i\xi x}d\xi \tag{2.13}$$

The integral in Equation (2.13) can be resolved analytically using the residues theorem and a semicircular contour in the complex ξ domain. We note that the integrant in Equation (2.13) has two poles, corresponding to the wavenumbers $-\xi_0$ and $+\xi_0$. We will resolve Equation (2.13) for the forward wave, which exists for $x > 0$ and generates a solution containing $i(\xi x - \omega t)$ in the exponential function. Hence, we will retain the positive pole, $+\xi_0$, inside the integration contour but exclude the negative pole, $-\xi_0$, from the integration contour. Using the residue theorem, the motion in the in-plane direction using wave propagation method is

$$u(x) = \frac{i}{2EA\xi_0}\left\{\hat{F}(-e^{-i\xi_0 x_0} + e^{-i\xi_0(x_0+l)})\right\}e^{i(\xi_0 x - \omega t)} \tag{2.14}$$

The flexural waves, the wave equation under harmonic excitation is

$$w'''' - \omega^2\frac{\rho A}{EI}w = g(x,t) \quad \text{where} \quad g(x,t) = \frac{1}{EI}\frac{h}{2}\left[\hat{F}\left[-\delta'(x-x_0) + \delta'(x-x_0-l)\right]\right] \tag{2.15}$$

Using the space-domain Fourier transform and residue theorem, the motion of the flexural vibration is

$$w(x) = -\frac{1}{4\xi_F^2}\frac{h}{2EI}\left[\hat{F}(-e^{-i\xi_F x_0} + e^{-i\xi_F (x_0+l)})\right]e^{i(\xi_F x-\omega t)} \tag{2.16}$$

Kinematic analysis gives the in-plane displacement of a generic point P on the beam surface in terms of the axial and flexural displacement as

$$u_P(t) = u(x) - \frac{h}{2}w'(x) = \frac{i\hat{F}}{2EA}\left\{\frac{(-e^{-i\xi_0 x_0} + e^{-i\xi_0 (x_0+l)})}{\xi_0}e^{i(\xi_0 x-\omega t)} + 3\frac{(-e^{-i\xi_F x_0} + e^{-i\xi_F (x_0+l)})}{\xi_F}e^{i(\xi_F x-\omega t)}\right\} \tag{2.17}$$

The elongation of PWAS is the difference of in-plane displacement of PWAS end, that is

$$\Delta u = u(x_0 + l) - u(x_0) = \hat{F}C_{AA}(\omega)e^{-i\omega t} \tag{2.18}$$

where the coefficient $C_{AA}(\omega)$ is

$$C_{AA}(\omega) = \frac{i}{2EA}\left(\frac{\left(e^{-i\xi_0 l} - 1\right)\left(e^{i\xi_0 l} - 1\right)}{\xi_0} + 3\frac{\left(e^{-i\xi_F l} - 1\right)\left(e^{i\xi_F l} - 1\right)}{\xi_F}\right) \tag{2.19}$$

2.5 Frequency Response Function

Under harmonic excitation, the FRF is the measure of any system's output spectrum in response to an input signal.

$$FRF(\omega) = \frac{OUT(\omega)}{IN(\omega)} \tag{2.20}$$

Under non-harmonic excitation, the instantaneous signal can be derived from the FRF. The instantaneous response can be calculated using the inverse Fourier transform of the product of excitation signal spectrum and FRF. Recall the convolution property of the Fourier transform, i.e.

$$out(t) = frf(t) * in(t) = \mathcal{F}^{-1}\left[FRF(\omega)IN(\omega)\right] \tag{2.21}$$

If the input voltage signal is an impulse function $in(t) = \delta(t)$, then the output voltage signal $out(t)$ is

$$out(t) = \int_{-\infty}^{\infty} frf(t-\lambda)in(\lambda)d\lambda = \int_{-\infty}^{\infty} frf(t-\lambda)\delta(\lambda)d\lambda = frf(t) \tag{2.22}$$

Hence, the response of the current signal to an impulsive input voltage signal is the impulse voltage response function of $frf(t)$. The function $frf(t)$ is called the impulse response function.

The admittance is defined as the frequency domain ratio of the current to the voltage. Giurgiutiu (2008) considered PWAS E/M impedance when PWAS was bonded on the structure. The E/M impedance measured at the PWAS is influenced by the dynamic stiffness $k_{str}(\omega)$ represented by the structure to the PWAS. The dynamic stiffness $k_{str}(\omega)$ is constraining the PWAS in its oscillation. The frequency–dependent stiffness ratio r is a function of frequency and is defined as the ratio $r = k_{str}(\omega)/k_i$. The $k_{str}(\omega)$ was defined as $k_{str}(\omega) = \hat{F}/\Delta u = 1/C_{AA}(\omega)$. The constrained PWAS admittance is

$$Y(\omega) = i\omega C_0\left[1 - k_{31}^2\frac{r(\omega)}{1+r(\omega)}\right] = i\omega C_0\left[1 - k_{31}^2\left(1 - \frac{k_i C_{AA}(\omega)}{k_i C_{AA}(\omega) - 1}\right)\right] \tag{2.23}$$

The FRF of pin-force at the end of PWAS is

$$FRF_{FV}(\omega) = \hat{F}(\omega)/\hat{V}(\omega) = \frac{1}{k_i C_{AA}(\omega) - 1}k_i d_{31}\frac{l}{t} \tag{2.24}$$

The FRF of velocity at PWAS end A and A' on the PWAS-structure interface is

$$FRF_{vVA}(\omega) = \frac{\hat{v}_A(\omega)}{\hat{V}(\omega)} = \frac{-\omega}{2EA}\left[\frac{1 - e^{-i\xi_0 l}}{\xi_0} + 3\frac{1 - e^{-i\xi_F l}}{\xi_F}\right]FRF_{FV}(\omega) \tag{2.25}$$

$$FRF_{vVA'}(\omega) = \frac{\hat{v}_{A'}(\omega)}{\hat{V}(\omega)} = \frac{\omega}{2EA}\left[\frac{1 - e^{i\xi_0 l}}{\xi_0} + 3\frac{1 - e^{i\xi_F l}}{\xi_F}\right]FRF_{FV}(\omega) \tag{2.26}$$

3. POWER AND ENERGY TRANSDUCTION

As PWAS transmitter, the active power, reactive power, power rating of electrical requirement under harmonic voltage excitation were examined. As PWAS receiver, the structural interface acoustic and electrical power and energy transduction were monitored under harmonic wave excitation. The parametric study of transmitter size and impedance, receiver size and impedance, and external electrical load gives the PWAS design guideline for PWAS sensing and power harvesting applications.

3.1 Transmitter Power and Energy

The input voltage provides the power from electrical source into piezoelectric power at the transmitter. Through piezoelectric transduction, electrical power converts to the mechanical interface power of the transmitter PWAS. The mechanical power at the interface becomes the acoustic wave power and the generated axial and flexural waves propagate in the structure.

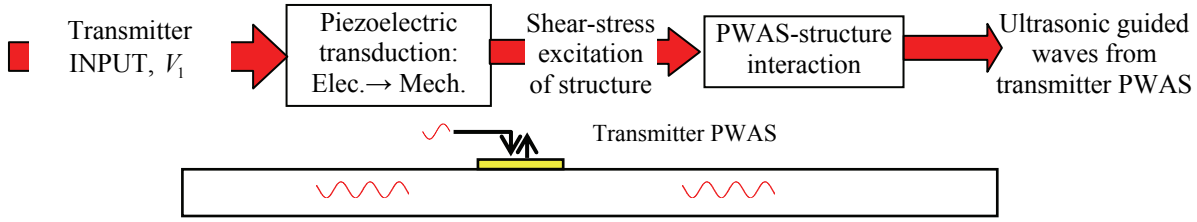

Figure 3 PWAS transmitter power and energy flow chart

Under harmonic excitation, the time-averaged power is the average amount of energy converted per unit time with continuous harmonic excitation. The time-averaged product of the two harmonic variables is one half the product of one variable times the conjugate of the other. When a harmonic voltage is applied to the transmitter PWAS, the current is

$$I = Y\hat{V} \tag{3.1}$$

The power rating, time-averaged active power and reactive power are

$$P_{rating} = \frac{1}{2}|Y|\hat{V}^2 = \sqrt{P_{active}^2 + P_{reactive}^2} \qquad P_{active} = \frac{1}{2}Y_R\hat{V}^2 \qquad P_{reactive} = \frac{1}{2}Y_I\hat{V}^2 \tag{3.2}$$

The active power is the power that converts to the mechanical power at the interface. The power rating is the power requirement of the power supply without distortion. In induced-strain transmitter applications, the reactive power is the dominant factor, since the transmitter impedance is dominated by its capacitive behavior. Managing high reactive power requirements is one of the challenges of using induced-strain transmitters.

The active electrical power provides the mechanical power at the interface through PWAS piezoelectric transduction. The mechanical power at the PWAS-structure interface are

$$\langle P_A \rangle = -\frac{1}{2}\bar{\hat{F}}(\omega)\hat{v}_A(\omega) = -\frac{1}{2}\overline{\left(FRF_{FV}(\omega)V(\omega)\right)}\left(FRF_{vVA}(\omega)V(\omega)\right) \tag{3.3}$$

$$\langle P_{A'} \rangle = \frac{1}{2}\bar{\hat{F}}(\omega)\hat{v}_{A'}(\omega) = \frac{1}{2}\overline{\left(FRF_{FV}(\omega)V(\omega)\right)}\left(FRF_{vVA'}(\omega)V(\omega)\right) \tag{3.4}$$

The simulation shows that the time-averaged mechanical power at the PWAS-structure interface both ends are equal, $\langle P_A \rangle = \langle P_{A'} \rangle$. The time-averaged active power equals the sum of the time-averaged interface mechanical power.

$$P_{active} = \langle P_A \rangle + \langle P_{A'} \rangle = 2\langle P_A \rangle \tag{3.5}$$

The mechanical power provides the power and energy for the generated axial and flexural waves. The analytical derivation shows that the time-averaged energy and power for the axial wave are

$$\langle e \rangle = \langle k \rangle + \langle v \rangle = \frac{1}{2}m\omega^2(u\,\bar{u}) \qquad \langle P_{axial} \rangle = c\langle e \rangle \tag{3.6}$$

Under the Euler-Bernoulli bending assumptions, the shear deformation and rotary inertia are ignored. The time-averaged flexural wave energy and power are

$$\langle e_F \rangle = \langle k \rangle + \langle v \rangle = \frac{1}{2}m\omega^2(w\,\bar{w}) \qquad \langle P_{flexural} \rangle = c_F\langle e_F \rangle \tag{3.7}$$

3.2 Receiver Power and Energy

Under strain wave $\varepsilon = \varepsilon_a e^{i(\xi_0 x-\omega t)} + \varepsilon_F e^{i(\xi_F x-\omega t)}$ travels to receiver PWAS at location x_0, the output voltage V can be calculated from Equation (2.8). The PWAS elongation under pin-force model gives

$$\Delta u = \varepsilon_a l\left(e^{i\xi_0(x_0+l)} - e^{i\xi_0 x_0}\right) + \varepsilon_F l\left(e^{i\xi_F(x_0+l)} - e^{i\xi_F x_0}\right) \tag{3.8}$$

The output voltage is calculated with the measurement equipment admittance

$$\hat{V} = \frac{1}{Y_e + (1-k_{31}^2)Y_0} i\omega b \frac{d_{31}}{s_{11}}\left(\varepsilon_a l\left(e^{i\xi_0(x_0+l)} - e^{i\xi_0 x_0}\right) + \varepsilon_F l\left(e^{i\xi_F(x_0+l)} - e^{i\xi_F x_0}\right)\right) \tag{3.9}$$

The time-average electrical output power for receiver is

$$\langle P(\omega)\rangle = \frac{1}{2}\mathrm{Re}\left(\overline{V}(\omega)I(\omega)\right) \quad \text{and} \quad I = Y_e V \tag{3.10}$$

Under axial strain $\varepsilon = \varepsilon_a e^{i(\xi_0 x-\omega t)}$ wave input, the mechanical power at receiver PWAS is

$$\langle P_A(\omega)\rangle = \frac{1}{2}\mathrm{Re}\left(\overline{F(\omega)}v_A(\omega)\right) \quad \text{where} \quad \hat{F} = R(\omega)k_t\Delta\hat{u} \text{ and } v_A = -i\omega\varepsilon_a l e^{i(\xi_0 x-\omega t)} \tag{3.11}$$

Under flexural strain $\varepsilon = \varepsilon_a e^{i(\xi_0 x-\omega t)}$ wave input, the mechanical power at receiver PWAS is

$$\langle P_A(\omega)\rangle = \frac{1}{2}\mathrm{Re}\left(\overline{F(\omega)}v_A(\omega)\right) \quad \text{where} \quad \hat{F} = R(\omega)k_t\Delta\hat{u} \text{ and } v_A = -i\omega\varepsilon_F l e^{i(\xi_F x-\omega t)} \tag{3.12}$$

3.3 Numerical Simulation

In simulation, an Aluminum alloy 2024 infinite bar with 40 mm width and 1 mm thickness was used. PWAS transmitter is 40mm width and 0.2 mm thickness. The transmitter size varies from 5 mm to 25 mm to show the trend of power consumption and wave power output. A 10V harmonic voltage is applied on the transmitter PWAS. The receiver size varies form 5mm to 25 mm. The external electrical load is fully resistive and varies from 1 Ω - 1 MΩ. Under constant harmonic voltage input, the voltage amplitude is 10V. Under constant power rating input, the power rating is 10 Watts. The frequency sweep range is from 1kHz to 600 kHz.

Table 1 Simulation Parameters

	Beam	Transmitter	Receiver
Length	∞	5-25 mm	5-25 mm
Height	1 mm	0.2 mm	0.2 mm
Width	40 mm		
Frequency	Frequency sweep 1 - 600 kHz		
Measurement Instrument Resistance	1 Ω - 1 MΩ		
Constant Voltage Input	10 V		
Constant Power Rating Input	10 Watts		

Under constant amplitude harmonic voltage input, the transmitter power rating is proportional with the transmitter admittance that is proportional to the PWAS size. The power rating vs. frequency and transmitter size is plotted in a 3D mesh plot (Figure 4 (a)). For a certain transmitter size, the power rating increases when the frequency increases. At a certain frequency, the power rating increases when the transmitter size increases. To drive a 25mm length PWAS at 600 kHz with 10 V constant voltage input, the power amplifier need to provide 12.5 W power. Figure 4b shows the total axial and flexural wave power that PWAS generates into the structure. The wave power output is determined by the tuning effect of transmitter size and excitation frequency. The maximum wave output in this experimental setup is about 40 mW. The active power is twice the wave power since the wave propagates in both directions. It shows that the reactive power is the dominant factor, since the transmitter impedance is dominated by its capacitive behavior. It also indicates the increasing the PWAS size solo does not mean to generate more wave power. It gives the guideline for the transmitter size and excitation frequency for maximum wave output. Figure 4c and d show the axial and flexural wave power separately under constant voltage input. In PWAS SHM applications, a single mode is often used to reduce the complexity. These Figures give the guideline for the optimum size and frequency for mode excitation.

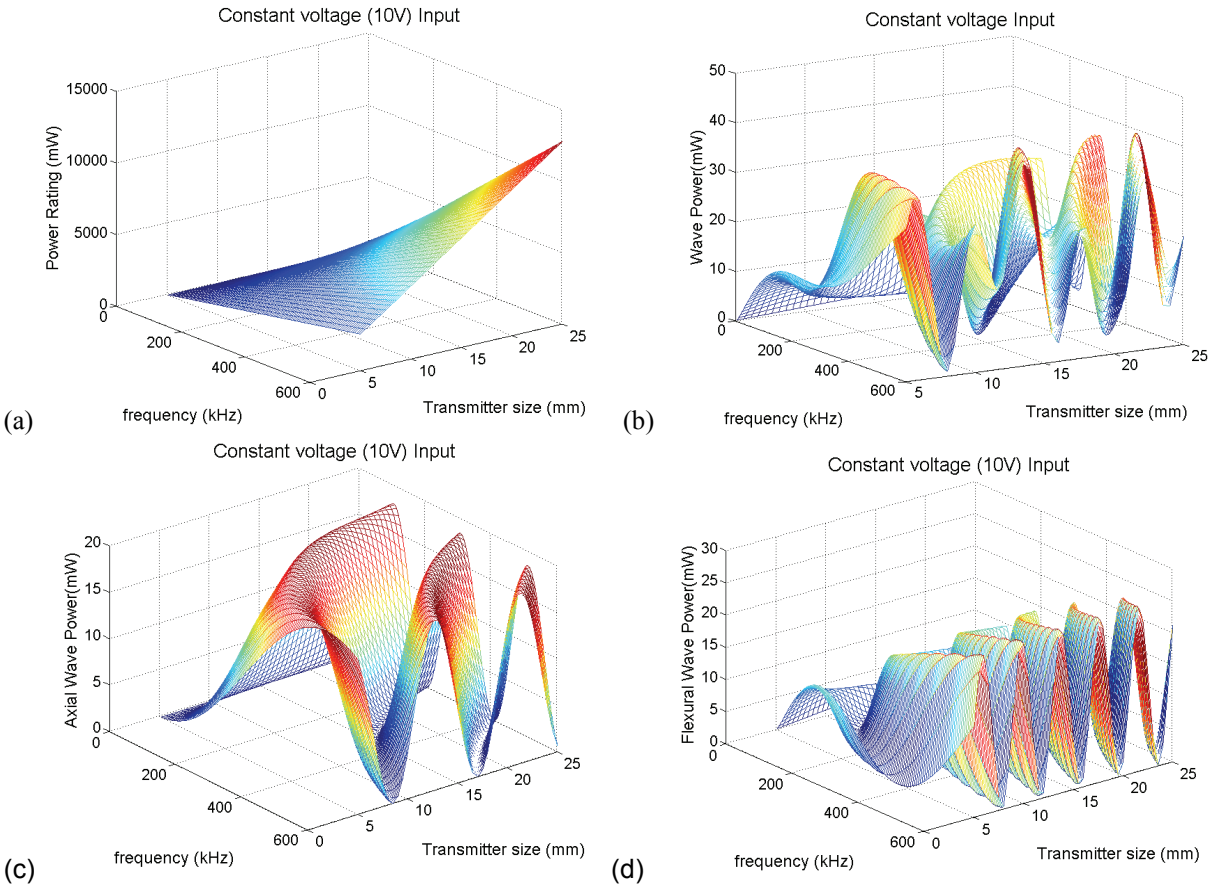

Figure 4 PWAS transmitter under constant voltage excitation (a) power rating; (b) wave power; (c) axial wave power; (d) flexural power

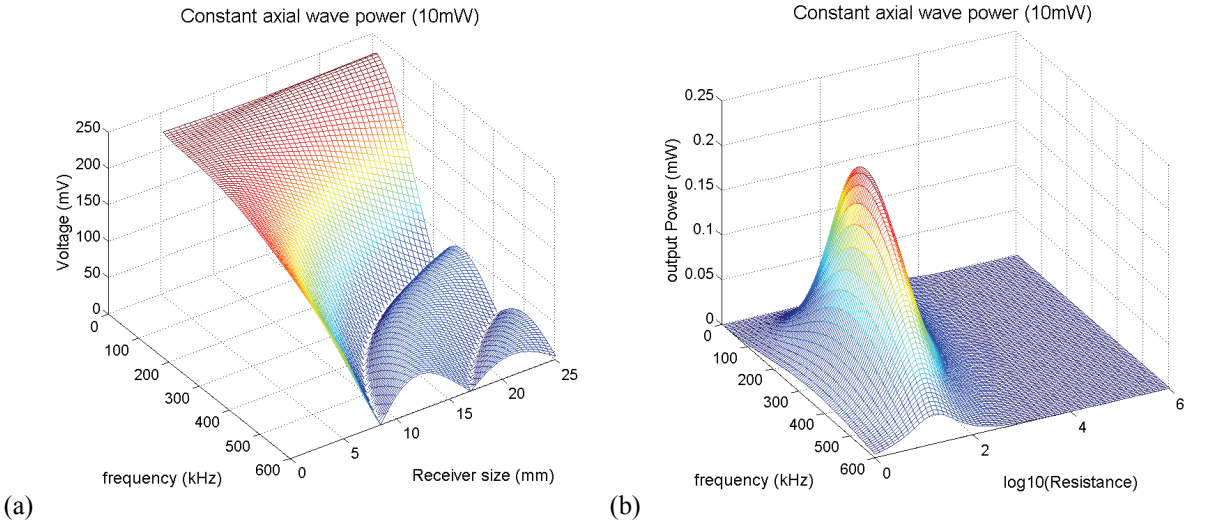

Figure 5 PWAS receiver under constant power of axial wave (a) Output voltage for sensing application; (b) Output power for power harvesting application

When propagating waves reach the receiver PWAS, receiver PWAS converts the wave energy to electrical energy and output voltage . For sensing application, the output voltage is of interest and expects high output voltage if possible. The external electrical load such as oscilloscope resistance is set to high impedance. The receiver size varies from 5mm to 25mm to show the sensing ability of different sensor size. At low frequency, PWAS receiver shows the similar ability of sensing regardless of PWAS size. The PWAS receiver sensing ability shows the tuning ability as we see the peak and valley in Figure 5a. In PWAS harvesting application, receiver size is fixed (e.g. 7 mm in simulation), the external electrical load impedance need to match the receiver impedance to output the maximum power. Considering a fully resistive external load varies from 1 Ω to 1 MΩ, the output electrical power is shown in Figure 5b. The optimum resistive load for power harvesting is around 100 Ω at 300 kHz for the 7 mm receiver PWAS.

4. PITCH-CATCH ANALYSIS

PWAS pitch-catch setup in 1-D model was shown in Figure 6. PWAS transmitter A with length l_A locates at location x_A , PWAS receiver B with length l_B locates at location x_B . Under ideal-bonding hypothesis, both PWAS A and B have pin-force at edges. The overall axial force and bending moment applied to the structure can be written as

$$N_e(x,t)=\left\{\hat{F}_A\left[-H(x-x_A)+H(x-x_A-l_A)\right]+\hat{F}_B\left[-H(x-x_B)+H(x-x_B-l_B)\right]\right\}e^{-i\omega t} \tag{4.1}$$

$$M_e(x,t)=-\left\{\frac{h}{2}\hat{F}_A\left[-H(x-x_A)+H(x-x_A-l_A)\right]+\frac{h}{2}\hat{F}_B\left[-H(x-x_B)+H(x-x_B-l_B)\right]\right\}e^{-i\omega t} \tag{4.2}$$

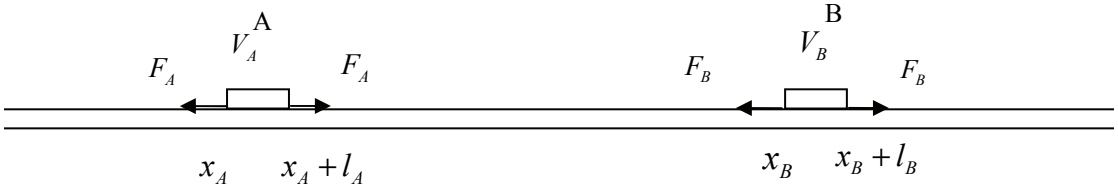

Figure 6 PWAS pitch-catch setup on an infinite bar

4.1 Pitch-catch Frequency Response Function

In pitch-catch setup, the axial force and bending moment is shown in Equation (4.1) and (4.2). The axial and flexural wave equations remain the same. The in-plane surface displacement can be solved using the space domain Fourier transform and residue theorem as well. The in-plane displacement of a generic point P on an infinite beam surface is

$$u_P(t)=\frac{i\hat{F}_A}{2EA}\left\{\begin{array}{l}\dfrac{(-e^{-i\xi_0 x_A}+e^{-i\xi_0(x_A+l_A)})}{\xi_0}e^{i(\xi_0 x-\omega t)}\\ +3\dfrac{(-e^{-i\xi_F x_A}+e^{-i\xi_F(x_A+l_A)})}{\xi_F}e^{i(\xi_F x-\omega t)}\end{array}\right\}+\frac{i\hat{F}_B}{2EA}\left\{\begin{array}{l}\dfrac{(-e^{-i\xi_0 x_B}+e^{-i\xi_0(x_B+l_B)})}{\xi_0}e^{i(\xi_0 x-\omega t)}\\ +3\dfrac{(-e^{-i\xi_F x_B}+e^{-i\xi_F(x_B+l_B)})}{\xi_F}e^{i(\xi_F x-\omega t)}\end{array}\right\} \tag{4.3}$$

The elongation of both PWAS A and B can be written as

$$\Delta u_A=(\hat{F}_A C_{AA}(\omega)+\hat{F}_B C_{BA}(\omega))e^{-i\omega t} \tag{4.4}$$

$$\Delta u_B=(\hat{F}_A C_{AB}(\omega)+\hat{F}_B C_{BB}(\omega))e^{-i\omega t} \tag{4.5}$$

where

$$C_{AA}(\omega)=\frac{i}{2EA}\left(\frac{\left(e^{-i\xi_0 l_A}-1\right)\left(e^{i\xi_0 l_A}-1\right)}{\xi_0}+3\frac{\left(e^{-i\xi_F l_A}-1\right)\left(e^{i\xi_F l_A}-1\right)}{\xi_F}\right) \tag{4.6}$$

$$C_{BA}(\omega)=\frac{i}{2EA}\left(\frac{e^{-i\xi_0(x_B-x_A)}\left(e^{-i\xi_0 l_B}-1\right)\left(e^{i\xi_0 l_A}-1\right)}{\xi_0}+3\frac{e^{-i\xi_F(x_B-x_A)}\left(e^{-i\xi_F l_B}-1\right)\left(e^{i\xi_F l_A}-1\right)}{\xi_F}\right) \tag{4.7}$$

$$C_{AB}(\omega)=\frac{i}{2EA}\left\{\frac{e^{-i\xi_0(x_A-x_B)}\left(e^{-i\xi_0 l_A}-1\right)\left(e^{i\xi_0 l_B}-1\right)}{\xi_0}+3\frac{e^{-i\xi_F(x_A-x_B)}\left(e^{-i\xi_F l_A}-1\right)\left(e^{i\xi_F l_B}-1\right)}{\xi_F}\right\} \tag{4.8}$$

$$C_{BB}(\omega)=\frac{i}{2EA}\left(\frac{\left(e^{-i\xi_0 l_B}-1\right)\left(e^{i\xi_0 l_B}-1\right)}{\xi_0}+3\frac{\left(e^{-i\xi_F l_B}-1\right)\left(e^{i\xi_F l_B}-1\right)}{\xi_F}\right) \tag{4.9}$$

Substitution of the transmitter pin-force and the elongation of PWAS equation (2.6) and the receiver pin-force and the elongation of PWAS equation (2.9) into (4.4) and (4.5), the elongation of PWAS Δu_A and Δu_B can be solved analytically. Using Equation (2.8), the output voltage of receiver PWAS can be derived. Notice the coefficient has the property $C_{AB}(\omega)C_{BA}(\omega)=C_{AA}(\omega)C_{BB}(\omega)$, the FRF of output voltage at PWAS B to the input voltage at PWAS A is

$$FRF_V(\omega)=\frac{V_B(\omega)}{V_A(\omega)}=\frac{k_{31}^2}{r_Y+(1-k_{31}^2)}\frac{k_{iA}C_{AB}(\omega)}{k_{iA}C_{AA}(\omega)+R(\omega)k_{iB}C_{BB}(\omega)-1} \tag{4.10}$$

For PWAS transmitter A, the FRF of admittance, pin-force and in-plane surface velocity used in electrical and mechanical power calculation are

$$Y(\omega)=\frac{\hat{I}}{\hat{V}_A}=i\omega C_0\left[1-k_{31}^2\left(1-\frac{k_{iA}C_{AA}(\omega)}{k_{iA}C_{AA}(\omega)+R(\omega)k_{iB}C_{BB}(\omega)-1}\right)\right] \tag{4.11}$$

$$FRF_{FVA}(\omega)=\frac{\hat{F}_A}{\hat{V}_A}=\frac{1-R(\omega)k_{iB}C_{BB}(\omega)}{k_{iA}C_{AA}(\omega)+R(\omega)k_{iB}C_{BB}(\omega)-1}k_{iA}d_{31}\frac{l_A}{t_A} \tag{4.12}$$

$$FRF_{FVB}(\omega)=\frac{\hat{F}_B}{\hat{V}_A}=\frac{k_{iA}C_{AB}(\omega)}{k_{iA}C_{AA}(\omega)+R(\omega)k_{iB}C_{BB}(\omega)-1}k_{iB}R(\omega)d_{31}\frac{l_A}{t_A} \tag{4.13}$$

$$FRF_{vVA}(\omega)=\frac{\hat{v}_A}{\hat{V}_A}=-\frac{\omega}{2EA}\left\{\left[\frac{1-e^{-i\xi_0 l_A}}{\xi_0}+3\frac{1-e^{-i\xi_F l_A}}{\xi_F}\right]FRF_{FVA}(\omega)+\left[\begin{array}{l}e^{-i\xi_0(x_B-x_A)}\dfrac{1-e^{-i\xi_0 l_B}}{\xi_0}\\ +3e^{-i\xi_F(x_B-x_A)}\dfrac{1-e^{-i\xi_F l_B}}{\xi_F}\end{array}\right]FRF_{FVB}(\omega)\right\} \tag{4.14}$$

$$FRF_{vVA'}(\omega)=\frac{\hat{v}_{A'}}{\hat{V}_A}=\frac{\omega}{2EA}\left\{\left[\frac{1-e^{i\xi_0 l_A}}{\xi_0}+3\frac{1-e^{i\xi_F l_A}}{\xi_F}\right]FRF_{FVA}(\omega)+\left[\begin{array}{l}e^{-i\xi_0((x_B+l_B)-(x_A+l_A))}\dfrac{1-e^{i\xi_0 l_B}}{\xi_0}\\ +3e^{-i\xi_F((x_B+l_B)-(x_A+l_A))}\dfrac{1-e^{i\xi_F l_B}}{\xi_F}\end{array}\right]FRF_{FVB}(\omega)\right\} \tag{4.15}$$

For PWAS receiver B, the FRF of in-plane surface velocity used in mechanical power calculation are

$$FRF_{vVB}(\omega)=\frac{\hat{v}_B}{\hat{V}_A}=-\frac{\omega}{2EA}\left\{\left[\begin{array}{l}e^{i\xi_0(x_B-x_A)}\dfrac{1-e^{-i\xi_0 l_A}}{\xi_0}\\ +3e^{i\xi_F(x_B-x_A)}\dfrac{1-e^{-i\xi_F l_A}}{\xi_F}\end{array}\right]FRF_{FVA}(\omega)+\left[\frac{1-e^{-i\xi_0 l_B}}{\xi_0}+3\frac{1-e^{-i\xi_F l_B}}{\xi_F}\right]FRF_{FVB}(\omega)\right\} \tag{4.16}$$

$$FRF_{vVB'}(\omega)=\frac{\hat{v}_{B'}}{\hat{V}_A}=\frac{\omega}{2EA}\left\{\left[\begin{array}{l}e^{i\xi_0((x_B+l_B)-(x_A+l_A))}\dfrac{1-e^{i\xi_0 l_A}}{\xi_0}\\ +3e^{i\xi_F((x_B+l_B)-(x_A+l_A))}\dfrac{1-e^{i\xi_F l_A}}{\xi_F}\end{array}\right]FRF_{FVA}(\omega)+\left[\frac{1-e^{i\xi_0 l_B}}{\xi_0}+3\frac{1-e^{i\xi_F l_B}}{\xi_F}\right]FRF_{FVB}(\omega)\right\} \tag{4.17}$$

4.2 Pitch-catch Power and Energy

The power and energy transduction flow chart for a complete pitch-catch setup is shown in Figure 7. Under 1-D assumption, the electro-acoustic power and energy transduction of the PWAS transmitter and receiver are examined. In pitch-catch mode, the power flow converts from electrical source into piezoelectric power at the transmitter, the piezoelectric transduction converts the electrical power into the mechanical interface power at the transmitter PWAS and then into acoustic wave power travelling in the structure. The wave power arrives at the receiver PWAS and is captured at the mechanical interface between the receiver PWAS at the structure, the mechanical power captured is

converted back into electrical power in the receiver PWAS and captured at the receivers electric instrument. The time-averaged electrical power, mechanical power at the transmitter and wave power can be calculated from the frequency response function. The time-averaged mechanical power and electrical power at the receiver PWAS can be calculated as well.

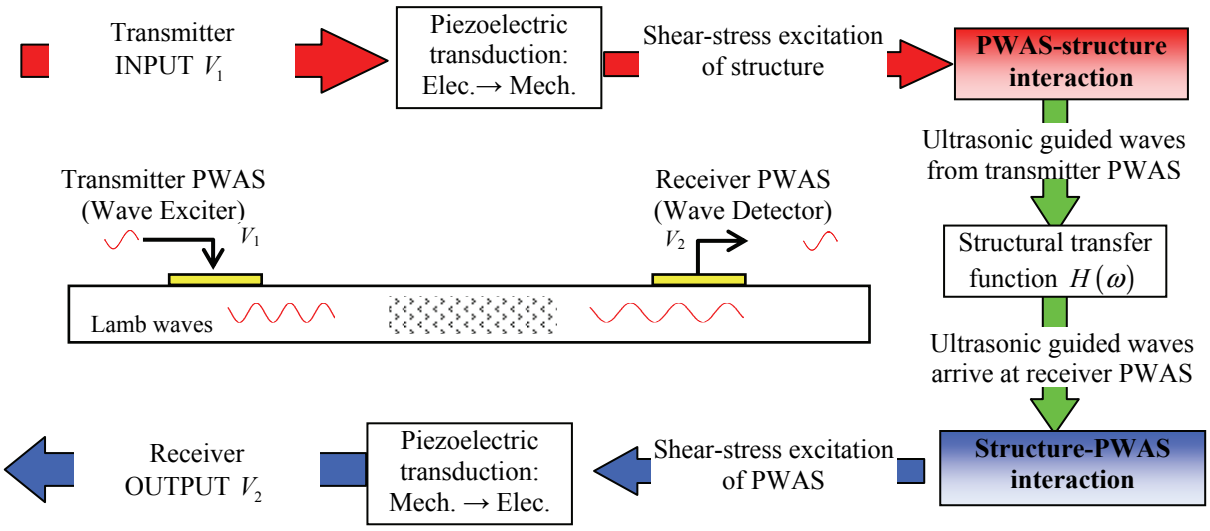

Figure 7 Pitch-catch power flow

4.3 Model verification

In pitch-catch setup simulation, an Aluminum alloy 2024 infinite bar was used with 40 mm width and 1 mm thickness. PWAS transmitter and receiver are 7-mm length, 40-mm width and 0.2-mm thickness. A 10V harmonic voltage is applied on the transmitter PWAS. The distance between transmitter and receiver is 200 mm.

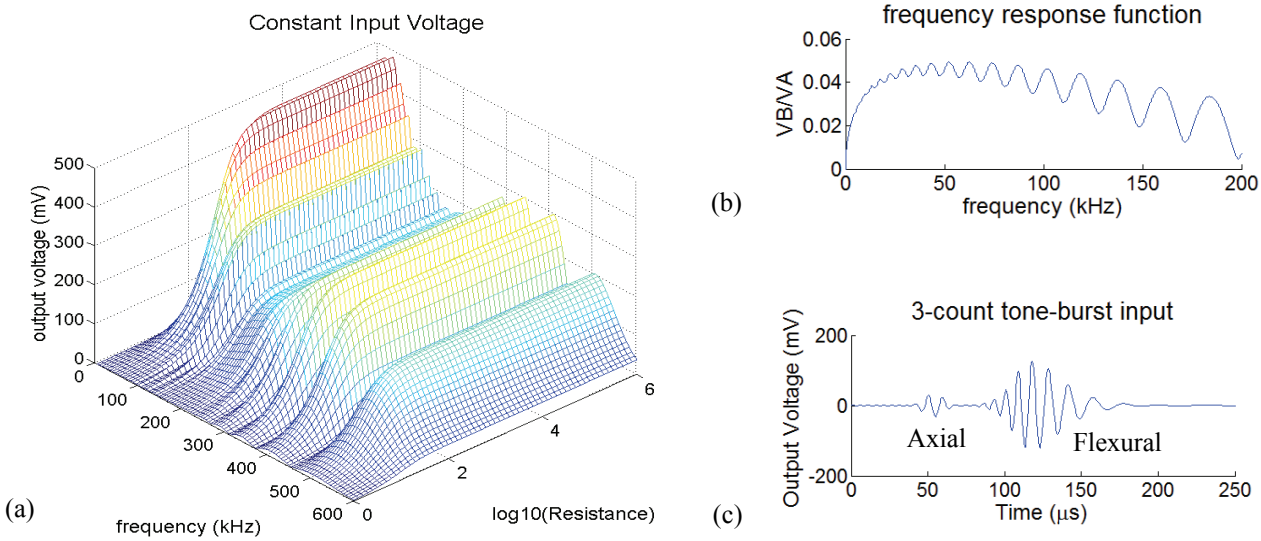

Figure 8 PWAS pitch-catch simulation under constant voltage input (a) Output voltage in relation of output resistance; (b) voltage output under harmonic excitation (c) voltage output under tone-burst excitation.

Figure 8a shows the output voltage of receiver PWAS when transmitter PWAS is excited by a harmonic constant amplitude (10V) input. The output electrical load varies. Figure 8b shows the frequency response function when the output electrical load is set at high Impedance (1 M Ω). A 100-kHz central frequency 3-count Hanning window tone-burst signal is applied to the transmitter. The receiver instantaneous voltage response is shown in Figure 8c. The fast axial wave is separated from the low speed flexural wave. The axial wave is non-dispersive and keep the shape of excitation signal. The flexural wave spread out due to the dispersive nature.

5. CONCLUSION AND FURTHER WORK

A systematic investigation of power and energy transduction in PWAS attached on structure was considered using the wave propagation methods. With 1-D wave propagation, ideal bonding and ideal excitation source assumption, frequency response function and power and energy transduction of PWAS transmitter and receiver were developed.

For PWAS transmitter, the active power, reactive power, power rating of electrical requirement were determined under harmonic voltage excitation. It indicates that the reactive power is dominant and gives the power requirement for power supply / amplifier for PWAS application. The electrical and mechanical power analysis at the PWAS structure interface indicates all the active electrical power provides the mechanical power at the interface. This provides the power and energy for the axial and flexural wave's power and energy travelling in the structure. Under 1-D wave propagation assumption, the axial and flexural waves propagate in both direction and the forward and backward waves power and energy are equal and the sum of forward and backward wave power equals the mechanical power PWAS applied to the structure. The parametric study of PWAS transmitter size shows the proper size and excitation frequency selection based on the tuning effects.

For PWAS receiver under harmonic strain excitation, the structure interface acoustic and electrical energy transduction was also developed. The parametric study of receiver size, receiver impedance and external electrical load gives the PWAS design direction for PWAS sensing and power harvesting application.

The power and energy flow of a complete pitch-catch setup was also considered. The electro-acoustic transduction of both PWAS transmitter and receiver are examined thoroughly. Both PWAS transmitter and receive pin-forces are considered for frequency transfer function and power and energy modeling. The power flow at each step in pitch-catch was monitored. The numerical simulation and graphical chart show the trends in the power and energy flow behavior with remarkable peaks and valleys that can be exploited for optimum design.

The future work is the power and energy analysis with assumptions in 2-D wave propagation and multi-mode Lamb waves.

6. ACKNOWLEDGMENTS

This material is based upon work supported by the National Science Foundation under Grant # CMS- 0925466, Shih-Chi Liu, Program Director and by the US Department of Commerce, National Institute of Standards and Technology, Technology Innovation Program, Cooperative Agreement Number 70NANB9H9007. Any opinions, findings, and conclusions or recommendations expressed in this material are those of the authors and do not necessarily reflect the views of the National Science Foundation or the US Department of Commerce, National Institute of Standards and Technology.

7. REFERENCES

1. ASCE, "Report Card for America's Infrastructure" , American Socienty of Civil Engineers, website http://www.asce.org/reportcard/2005/index.cfm
2. Viktorov, I. A. (1967) Rayleigh and Lamb Waves – Physical Theory and Applications, Plenum Press, NY,1967
3. Auld, B. A. (1990) Acoustic Fields and Waves in Solids, Wiley Interscience, John Wiley & Sons, Vol. 1 and 2, 1973
4. Achenbach, J. D. (1973) Wave Propagation in Elastic Solids, Elsevier, 1973
5. Rose, J. L. (1999) Ultrasonic Waves in Solid Media, Cambridge University Press, New York, 1999
6. Giurgiutiu, V. (2008) *Structural Health Monitoring with Piezoelectric Wafer Active Sensors*, Elsevier Academic Press, 760 pages, 2008, ISBN 978-0120887606
7. Giurgiutiu, V. (2009) *Micromechatronics Modeling, Analysis, and Design with MATLAB (second edition)*, CRC Press, 920 pages, 2009, ISBN 978-1-4200-6562-6
8. Graff, K. F. (1975) *Wave Motion in Elastic Solids*, Oxford University Press, 649 pages, 1975, ISBN 0-486-66745-6